Spin reorientation in $NdFe_{0.5}Mn_{0.5}O_3$: Neutron scattering and *ab initio* study

Ankita Singh,[1] A. Jain,[2,3] Avijeet Ray,[1] Padmanabhan B.,[1] Ruchika Yadav,[4] Vivian Nassif,[5,6,7] Sajid Husain,[8] S. M. Yusuf,[2,3] T. Maitra,[1,*] and V. K. Malik[1,†]

[1]*Department of Physics, Indian Institute of Technology Roorkee, Roorkee 247 667, India*
[2]*Solid State Physics Division, Bhabha Atomic Research Center, Mumbai 400 085, India*
[3]*Homi Bhabha National Institute, Anushaktinagar, Mumbai 400 094, India*
[4]*Laboratory for Scientific Developments and Novel Materials, Paul Scherrer Institut, CH-5232 Villigen, Switzerland*
[5]*Université Grenoble-Alpes, Institut Néel, 25 Avenue des Martyrs-BP166, 38042 Grenoble, cedex 9 France*
[6]*Centre Nationale de la Recherche Scientifique, Institut Néel, 25 Avenue des Martyrs-BP166, 38042 Grenoble, cedex 9 France*
[7]*Institut Laue -Langevin, 71 Avenue des Martyrs, 38000 Grenoble, cedex 9 France*
[8]*Thin Film Laboratory, Department of Physics, Indian Institute of Technology Delhi, New Delhi 110 016, India*

(Received 1 February 2017; revised manuscript received 27 July 2017; published 17 October 2017)

The structural, magnetic, and electronic properties of $NdFe_{0.5}Mn_{0.5}O_3$ have been studied in a comprehensive manner using various experimental and theoretical methods. Mn/Fe sublattice of the compound orders into a G-type antiferromagnetic phase close to 250 K where the magnetic structure belongs to Γ_1 irreducible representation (G_y) unlike Γ_4 (G_x) representation observed in most of the orthoferrites and orthochromites. The magnetic structure undergoes a complete spin reorientation transition with temperature between 75 and 25 K where the magnetic structure exists as a sum of two irreducible representations ($\Gamma_1 + \Gamma_2$). At 1.5 K, the antiferromagnetic structure belongs entirely to Γ_2 representation (G_z) with a small ferromagnetic component (F_x) due to Nd. The unusual spin reorientation and correlation between magnetic ground state and electronic structure have been investigated using phenomenological theory and first-principles calculations within GGA+U and GGA+U+SO formalisms.

DOI: 10.1103/PhysRevB.96.144420

I. INTRODUCTION

Ferromagnetic materials have been utilized extensively for practical applications starting from 200 BC as compasses till recently as information storage and read/write devices [1–3]. Such versatile applications of ferromagnetic materials have been feasible by virtue of easy manipulation of magnetization utilizing moderate magnetic fields [4]. On the other hand, antiferromagnetic ordering is difficult to control through an external magnetic field and found limited applications as a pinning layer for adjacent ferromagnetic layers in read heads of storage devices [5]. Rapid generation of digital data requires enhancement of the data storage density and speed of the data transfer. The latter is specifically limited by the time scale of magnetization manipulation (∼10 ns) due to slow decay and rise time of magnetic fields in present data storage devices [1]. Novel methods to manipulate magnetic order using ultrashort (∼picoseconds) pulses of coherent electromagnetic radiation have unwrapped the possibilities for development of faster storage devices having manipulation time at (sub)picosecond scale [1,6].

Rare-earth (RE) orthoferrites, from a family of strongly correlated materials, exhibit two orders of magnitude faster spin dynamics in comparision to conventional ferromagnetic materials [7,8]. Most of the RE orthoferrites ($RFeO_3$) are G-type canted antiferromagnets with a weak ferromagnetic component due to Dzyaloshinskii-Moriya (DM) interaction and show temperature-induced spin reorientation from one magnetic symmetry to another. Exchange interactions between Fe^{3+}-Fe^{3+}, R^{3+}-Fe^{3+}, and R^{3+}-R^{3+} play an important role to determine the complex magnetic properties (e.g., magnetic structure and spin reorientation) of $RFeO_3$. Isotropic Fe^{3+}-Fe^{3+} exchange interaction dictates the magnetic structure of Fe^{3+} spins below ordering temperature (T_N). Exchange field due to Fe^{3+} moment on R sublattice polarizes the R^{3+} spins. Further, comparatively weaker anisotropic exchange interaction between R^{3+} and Fe^{3+} generate effective fields on Fe^{3+} spins, which in turn start to rotate and try to align perpendicular to R^{3+} spins. This transition might be continuous/abrupt depending upon the RE element [9].

$NdFeO_3$ is one of the well studied family members of orthoferrite materials, which exhibits antiferromagnetic ordering and temperature dependent spin reorientation [10–25]. It crystallizes in orthorhombic crystal structure of the space group $Pbnm$ and comprises of distorted corner shared FeO_6 octahedra. $NdFeO_3$ is a canted G-type antiferromagnet with a high Néel temperature (T_N) of 690 K [20]. The magnetic structure is represented as G_xF_z belonging to irreducible representation Γ_4, in which the spins form a G-type antiferromagnetic order along a direction (G_x), with a small ferromagnetic component along c direction due to canting (F_z). As the temperature is lowered, Fe spins rotate continuously in ac plane in the temperature range 200 to 105 K resulting in a change in the magnetic configuration from G_xF_z of Γ_4 to F_xG_z of Γ_2 representation with G-type ordering along the c direction (G_z) and a weak ferromagnetic ordering in the a direction (F_x) [15]. Though the whole process of spin reorientation is quite complex, a noticeable ordering of Nd moments as C-type antiferromagnet emerges at 1.5 K [17–19]. The weak ferromagnetic moments, F_x of Fe and f_x of Nd, in $NdFeO_3$ single crystals are antiparallel and the overall spontaneous magnetization is compensated at $T = 8$ K [23]. $NdFeO_3$ could be utilized in high frequency electronic components owing to its large band gap (∼2.5 eV).

*tulimfph@iitr.ac.in
†vivekfph@iitr.ac.in

Another RE transition metal oxide which has drawn considerable attention for its intriguing properties is $NdMnO_3$. $NdMnO_3$ is A-type antiferromagnet with relatively low T_N of 75 K [26]. Although $NdMnO_3$ and $NdFeO_3$ are isostructural and antiferromagnetic, the underlying mechanism responsible for their complex magnetic properties is quite different. In $NdMnO_3$, the Mn ion has 3+ oxidation state with $3d^4$ electronic configuration, which splits under crystal field into low lying triply degenerate t_{2g} states and doubly degenerate e_g states at higher energies [27,28]. The doubly degenerate e_g is split into e_g^1 and e_g^2 states due to the Jahn-Teller (J-T) distortion, which is also manifested as structural distortion. This results in tilting of octahedra by $\sim 45^\circ$ in a zigzag manner and also compression of the in-plane Mn-O bonds and elongation of the apical Mn-O bond. As a consequence of crystal field splitting and co-operative J-T effect, the highest occupied e_g orbital orders as $d_{3x^2-r^2}$ and $d_{3y^2-r^2}$ alternately at adjacent Mn sites in the ab plane [29]. Such a staggered in-plane orbital ordering leads to a ferromagnetic alignment of spins in ab plane and antiferromagnetic alignment along the c direction resulting in A-type antiferromagnetic structure below T_N ($\sim$75 K) [26]. As the temperature is further reduced, the Nd sublattice orders ferromagnetically along the a direction below 20 K [29,30]. The ordered Nd moment induces a Mn spin reorientation and a negative magnetization in $NdMnO_3$ [30]. The electronic properties of this system fall in an intermediate regime between a Mott insulator and charge transfer insulator with a band gap of about 1 eV primarily due to J-T distortion. This has been studied from density functional theory based band structure calculations [31].

In view of the very different magnetic properties shown by $NdFeO_3$ and $NdMnO_3$, it would be extremely interesting to look at an intermediate system where we substitute half of the Fe ions with Mn. In this situation, one would expect a very complex interplay of spin, lattice, and orbital degrees of freedom between the Mn and Fe sublattices and hence a new set of enriching physical properties. Substitution of Mn^{3+} ions at the Fe site not only makes it J-T active, it also tunes the superexchange interaction, influences the magnetic symmetry, and spin reorientation through the Mn-Fe, Nd-Mn, and Nd-Fe interactions [32–34]. The electron-phonon coupling will also change due to change in J-T interaction upon substitution. Troyanchuk *et al.* [34] studied 50 % substitution of Mn at Fe site using neutron diffraction at 4.3 K. Magnetic structure was found to be G-type at 4.3 K. However, the authors did not provide any information about the direction of magnetic moments.

In the present work, we have studied the effect of 50% Mn substitution at Fe sites on the magnetic structure, spin reorientation, and electronic structure of $NdFe_{0.5}Mn_{0.5}O_3$ (NFMO). We have used various experimental techniques, viz. x-ray diffraction, magnetization, neutron diffraction, neutron depolarization, and also theoretical techniques such as density functional theory calculations to establish the complex magnetic structure of NFMO compound as well as to understand the underlying mechanism. A unique magnetic symmetry Γ_1 (G_y) was observed below (T_N), which transforms gradually into a commonly observed symmetry Γ_2 (G_z) through a spin reorientation transition with temperature. To the best of our knowledge, the Γ_1 symmetry has not been observed previously above spin reorientation transition temperature in the family of orthoferrites. The observation of two magnetic structures and spin reorientation in NFMO has been explained on the basis of magnetic anisotropy energy calculated using first-principles calculations.

II. METHODS

A. Experimental

Powder sample of NFMO was synthesized using a standard solid state reaction method. Nd_2O_3, MnO_2, and Fe_2O_3 were weighed according to appropriate stoichiometry and ground in an agate mortar for 12 hours. The heat treatment of the sample was carried out according to the procedure explained in Ref. [35]. The structural phase of the sample was identified using a Bruker D8 two-circle x-ray diffractometer at Cu K_α wavelength. Average magnetization measurements were performed using a vibrating sample magnetometer (VSM) module of the Quantum Design make Physical Property Measurement System (QD-PPMS) Evercool-II. Further measurements were repeated using superconducting quantum interference device (SQUID) of Quantum Design Magnetic Property Measurement System (MPMS) to confirm the results obtained from VSM. Zero-field cooled (ZFC) and field cooled (FC) measurements from 350 to 10 K in 0.01 T magnetic field were carried out to identify the different magnetic transitions and their respective temperatures. Field variation of magnetization was carried out at various temperatures between 300 and 5 K. Neutron diffraction studies in absence of magnetic field were carried out at various temperatures in the range of 1.5–300 K to identify the crystal as well as magnetic structures and their variations as a function of temperature. Neutron diffraction measurements were carried out using powder diffractometers PD-I ($\lambda = 1.094$ Å) and PD-II ($\lambda = 1.2443$ Å) at the Dhruva reactor, Trombay, Mumbai, India. High resolution neutron diffraction measurements were performed at D1B(CRG)-high resolution two-axis neutron powder diffractometer ($\lambda = 2.524$ Å), Institut Laue-Langevin, Grenoble, France. The diffraction data were analyzed using the FULLPROF [36] suite of programs employing the Rietveld method [37]. Magnetic structure was determined using the irreducible representations from BASIREPS [38], and refined using FULLPROF. One dimensional neutron depolarization measurements over the temperature range of 4–300 K, to identify the short-range weak ferromagnetism, were carried out using the polarized neutron spectrometer (PNS) at the Dhruva reactor, under an applied magnetic guide field of 50 Oe. For the neutron depolarization measurements, polarized neutrons ($\lambda = 1.205$ Å) were produced and analyzed by using magnetized Cu_2MnAl (111) and $Co_{0.92}Fe_{0.08}$ (200) single crystals, respectively [39,40]. The two different states (up and down) of the incident neutron beam polarization were achieved by a π flipper just before the sample. The polarization of the neutron beam was determined by measuring the intensities of neutrons in non-spin flip and spin flip channels with the flipper off and on (flipping ratio, R), respectively.

B. Theoretical

Electronic structure of NFMO was obtained using the projector-augmented wave (PAW) psuedopotential and a

plane-wave basis method within the density functional theory framework as implemented in the Vienna *ab initio* simulation program (VASP) [41]. Calculations are performed within the Perdew-Burke-Ernzerhof generalized gradient approximation (PBE-GGA) [42] and GGA+U [43]. Noncollinear magnetic calculations were performed within the GGA+U+SO approximation. The Mn(Fe) $3d$,$4s$; O $2s$,$2p$; and Nd $5p$,$5d$,$6s$ states were treated as valence states. An energy cutoff of 400 eV was used for the plane-wave basis set while a $6\times6\times6$ Monkhorst-Pack k mesh centered at Γ was used for performing the Brillouin zone integrations. Ionic positions were relaxed until the forces on the ions are less than 0.1 meV $Å^{-1}$. The calculations were performed for different magnetic configurations viz. ferromagnetic, A, C, and G-type antiferromagnetic configurations.

III. EXPERIMENTAL RESULTS

A. Structural characterization

Figure 1 shows the room-temperature x-ray diffraction pattern of the NFMO powder sample. Orthorhombic structure of the sample, as reported for the end members $NdFeO_3$ [20] and $NdMnO_3$ [44,45], has been considered for refinement shown in Fig. 1. The preliminary analysis of the x-ray diffraction data confirms the phase formation and purity of the NFMO sample. The mixed doped NFMO compound can be considered as double perovskite Nd_2FeMnO_6 with B-site ordering of Mn and Fe ions. B-site ordering of the compound should mark the unique positions for transition metal ions which results in monoclinic structure. Random occupation of B site by transition metal ions leads to the orthorhombic crystal structure. The diffraction pattern was refined to orthorhombic ($Pbnm$) as well as monoclinic ($P2_1/n$) space groups with comparable χ^2 values. Hence it is not possible to confirm the crystal structure using x-ray diffraction alone. However, our attempts to find traces of weak (021) Bragg peak, which should occur only in monoclinic structure, did not succeed because of similar scattering factors of Mn and Fe. Besides the observed magnetic behavior is entirely different from that expected from a double perovskite compound which predominantly show ferromagnetism, e.g., in R_2MnBO_6 (R=La,Nd and B=Ni,Co) [46–49]. This information indicates the possible phase formation of NFMO with the orthorhombic symmetry. However, the structure could be confirmed using neutron diffraction measurements. Unlike x-ray diffraction, the scattering lengths of Mn (-3.73×10^{-15}) and Fe (9.94×10^{-15}) are different in case of neutron diffraction. This distinction helps to identify the B-site order/disorder. Figure 2 shows measured and refined neutron diffraction patterns of NFMO for 300 K at PD-II using neutron wavelength of 1.2443 Å. The diffraction pattern was fitted to orthorhombic structure as shown in Fig. 2, which shows excellent agreement with the experimental pattern. However, the monoclinic structure gives a much poorer quality of fitting (not shown) unlike the x-ray pattern. Thus it can be concluded that NFMO crystallizes in the orthorhombic space group and the Mn/Fe atoms are arranged in a random manner at the $4b$ Wyckoff positions.

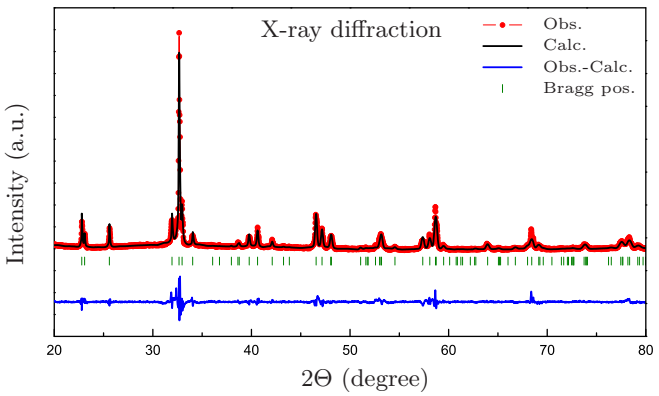

FIG. 1. Observed x-ray diffraction pattern of NFMO at room temperature, refined using orthorhombic $Pbnm$ space group.

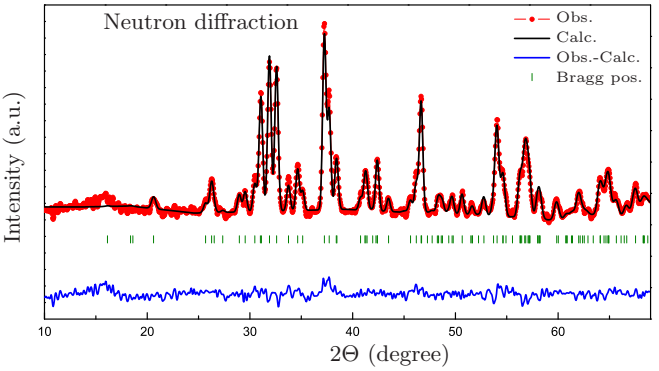

FIG. 2. Observed and refined neutron diffraction patterns of NFMO at room temperature confirm formation of the orthorhombic structure with $Pbnm$ space group. The measurement was performed at PD-II using neutron wavelength of 1.2443 Å.

In this section, we compare the structural parameters of NFMO (obtained form the present study) with those reported in literature for $NdFeO_3$ [20] and $NdMnO_3$ [45]. In Table I, the lattice constants along with M-O(M = Fe, Mn) bond lengths of $NdFe_{0.5}Mn_{0.5}O_3$ have been shown for 300, 90, and 1.5 K. We observe that the lattice parameters (a and c) of $NdFeO_3$ are larger than those of NFMO while b of $NdMnO_3$ is larger than that of NFMO. Thus the lattice parameters of NFMO are intermediate, though we find that the values of b and c are closer to that of $NdFeO_3$ ($\Delta a = -0.38\%, \Delta b = +0.17\%, \Delta c = -0.75\%$), while a is closer to that of parent manganite $NdMnO_3$ ($\Delta a = +0.24\%, \Delta b = -4\%, \Delta c = +1.93\%$). We note the large changes in b and c lattice parameters in comparison to $NdMnO_3$. These values are also in good agreement with recent work done by Chakraborty *et al.* on a series of $NdFe_{1-x}Mn_xO_3$ samples [35]. In case of $RMn_xFe_{1-x}O_3$ (R = RE element), it has been observed that the long-range cooperative (static) J-T distortion is effective for higher values of x (>0.8) and the structure is classified as O′-orthorhombic with $c/\sqrt{2} < a < b$ in this regime. Static J-T distortion disappears for $x \leqslant 0.8$ and structure changes into O-orthorhombic with $a < c/\sqrt{2} < b$. A weaker orbital ordering associated with dynamical J-T effect at Mn sites may still be present in the system down to $x \approx 0.5$ [35,50,51]. This inequality $a < c/\sqrt{2} < b$ is also observed in case of NFMO with a small difference between a and $c/\sqrt{2}$.

TABLE I. Structural parameters of $NdFe_{0.5}Mn_{0.5}O_3$ in comparison to $NdMnO_3$ and $NdFeO_3$ [20,45].

Compound	$NdFe_{0.5}Mn_{0.5}O_3$			$NdMnO_3$	$NdFeO_3$
Parameters	300 K	90 K	1.5 K	295 K	295 K
a(Å)	5.4303(5)	5.4205(2)	5.4198(2)	5.4170	5.4510
b(Å)	5.6039(6)	5.6066(3)	5.6067(3)	5.8317	5.5880
c(Å)	7.7038(9)	7.6806(4)	7.6788(2)	7.5546	7.7616
Mn(Fe)-O(1)(m) Å	1.9897(8)	1.9843(9)	1.9834(9)	1.951	2.0012
Mn(Fe)-O(2)(l) Å	2.0543(19)	2.0576(23)	2.0555(24)	2.218	2.0226
Mn(Fe)-O(2)(s) Å	1.9659(20)	1.9648(22)	1.9670(26)	1.905	2.0072
Mn(Fe)-Mn(Fe)(p) Å	3.8519(15)	3.8990(5)	3.8394(9)	3.9342	3.8810
Mn(Fe)-Mn(Fe)(o) Å	3.9016(10)	3.8990(5)	3.8990(5)	3.7945	3.9031
		Present study		Ref. [45]	Ref. [20]

Three different M-O bond lengths have been listed in Table I. Long (l) and short (s) bond lengths correspond to the M-O(2) bonds in the ab plane. Medium (m) bond length corresponds to the out of plane M-O(1) apical bond which is almost parallel to the c axis. These three different bond lengths are depicted in Fig. 10(a) for clarity. In $NdFeO_3$, l, m, and s are almost equal implying that the distortion of the octahedra is minimal. While in $NdMnO_3$, the bond lengths are highly unequal due to the J-T distortion associated with orbital ordering in the ab plane. In NFMO, it is expected that the Mn-O and Fe-O bond lengths should be unequal. However, only average bond lengths for the three M-O bonds are obtained experimentally. Comparing the M-O bond lengths of NFMO with $NdFeO_3$, a slight decrease in s and an increment in l, m is observed. Though the changes are minimal, it indicates possibility of the J-T distortion in the ab plane. The in-plane and out-of-plane distortions are characterized by the J-T parameters $Q_2 = 2(l-s)/\sqrt{2}$ and $Q_3 = 2(2m-l-s)/\sqrt{6}$ respectively [45]. Here, Q_2 is associated with in-plane J-T distortion, while Q_3 is an indicator of the out-of-plane tetragonal distortion. Values of Q_2 and Q_3 are nearly zero in case of $NdFeO_3$. For NFMO, we find that at 300 K, $Q_2 = 0.125$ and $Q_3 = -0.0331$, as obtained using bond lengths from Table I. In this case (NFMO), both the distortion parameters are nonzero, but are much smaller compared to $NdMnO_3$ ($Q_2 = 0.4426$ and $Q_3 = -0.1797$). Thus the in-plane J-T distortion appears stronger than the out-of-plane tetragonal distortion. An additional parameter often used to quantify the distortion of the octahedra is Δ_d defined as $\Delta_d = (1/6)\Sigma_{n=1,6}[(d_n - \langle d\rangle)/\langle d\rangle]^2$ [45], where d_n's are the individual M-O bond lengths. In case of NFMO, we observe that the level of octahedral distortion ($10^4\Delta_d = 3.47$) is smaller by an order of magnitude in comparison to $NdMnO_3$ ($10^4\Delta_d = 46.4$), but higher than $NdFeO_3$ ($10^4\Delta_d = 0.2$). Due to the presence of long-range static J-T effect and orbital ordering, such high level of octahedral distortions are seen to exist in $NdMnO_3$ [35].

In case of NFMO, the temperature variation (not shown) of lattice parameters a and c is quite similar to that of $NdFeO_3$. However, the parameter b shows a continuous increase with decreasing temperature till 90 K beyond which it is nearly constant. This is unlike in $NdFeO_3$, which shows an initial decrease till 150 K and then continuously rises till 4 K [20]. For NFMO, the increase in b can also be linked with the variation of the M-O(2)(l) bond lengths with temperature and possible increase in J-T distortion at Mn sites. Similarly, the medium bond length (m) shows a systematic decrease with temperature as shown in Table I. However, l shows an overall increase with decreasing temperature, though it shows a higher value for 90 K compared to 1.5 K, indicating a possible reduction in J-T distortion below 90 K. Presence of a dynamical J-T effect associated with a weak and short-range orbital ordering in NFMO could be inferred from the above mentioned facts about lattice constants, bond lengths, J-T parameter and temperature dependent data.

B. Magnetic properties

1. dc magnetization

As shown in Fig. 3, ZFC and FC magnetization measurements were performed from 2 to 350 K in the magnetic field of 10 mT. Temperature dependent ZFC and FC show a characteristic cusp (see inset of Fig. 3) at 250 K denoting an antiferromagnetic ordering of the M (Mn/Fe) spins. The parent compound $NdFeO_3$ undergoes from paramagnetic state to G-type antiferromagnetic state at 690 K [20]. As recently reported by Chakraborty *et al.* [35], T_N is seen to decrease systematically with increase of Mn substitution in $NdFe_{1-x}Mn_xO_3$.

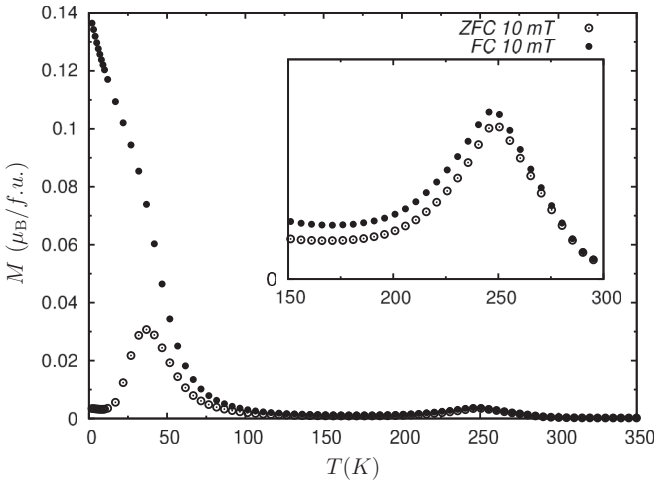

FIG. 3. ZFC-FC plots of NFMO from 2 to 350 K showing Néel temperature (T_N) at 250 K and weak ferromagnetism below 70 K.

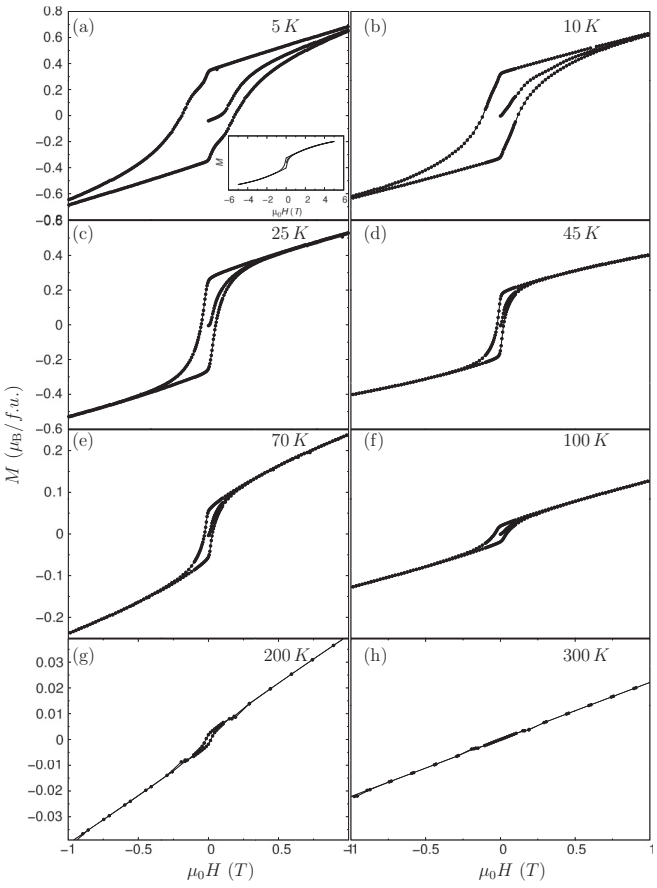

FIG. 4. M-H plots of NFMO at (a) 5, (b) 10, (c) 25, (d) 45, (e) 70, (f) 100, (g) 200, and (h) 300 K.

Since the value of T_N is 622 K for $x = 0.1$, 529 K for $x = 0.2$, 449 K for $x = 0.3$, and 356 K for $x = 0.4$ in $NdFe_{1-x}Mn_xO_3$ [52]; therefore, the observed value of T_N (250 K) for NFMO is consistent with previous reports. ZFC and FC magnetization exhibit an increase below 70 K, and a large bifurcation below 37 K. ZFC magnetization decreases below 37 K, whereas FC magnetization keeps increasing with a slight change in slope at 37 K. Such magnetization is observed typically for spin glass systems, weak ferromagnetic systems, and systems with short-range magnetic correlations [53]. FC magnetization does not follow the mean-field magnetization for a ferromagnet with long-range ordering. Troyanchuk *et al.* [34] attributed the low-temperature magnetic behavior in NFMO entirely to a spin glass state. However, frequency-dependent ac-susceptibility measurements ruled out the presence of a spin glass state in the present study (data not shown). Further, magnetization (M) versus magnetic field (H) loops were measured at various temperatures to understand the low-temperature magnetic behavior (below 70 K) of NFMO.

The magnetization isotherms (M-H loops) of NFMO at various temperatures from 5 till 300 K have been shown in Fig. 4. At 300 K, the magnetization isotherm shows a linear behavior without any hysteresis as expected from a majority paramagnetic phase. At 200 and 100 K, the M-H loops are quite similar having a deviation from the linear behavior with a small coercivity, retentivity, and unsaturated magnetization, which is usually seen predominantly in antiferromagnetic

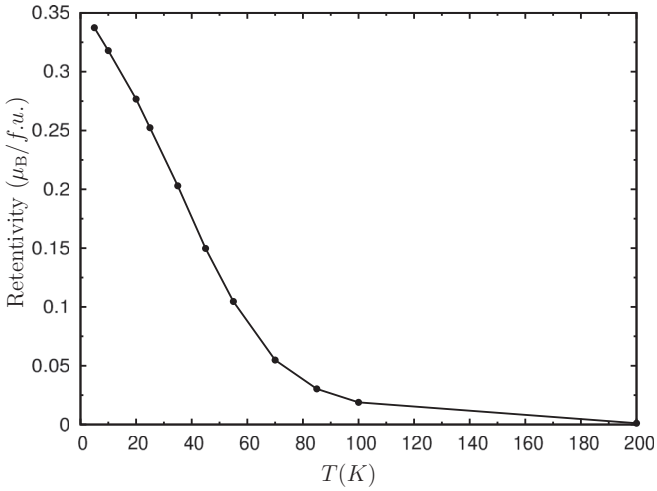

FIG. 5. Variation of retentivity with temperature in NFMO.

materials. The nature of M-H loops below 70 K changes considerably (both qualitatively and quantitatively) with an increase in coercivity and retentivity. Another qualitative change in the M-H loop occurs below 25 K with a large coercivity value. The shape of the M-H loops obtained at 10 and 5 K is significantly different from the loops measured at 25, 45, and 70 K. The M-H loops below 100 K indicate development of a ferromagnetic component. However, the magnetization does not undergo saturation even at 5 K in a field of 5 T as seen in the inset of Fig. 4(a), indicative of a ferromagnetic component superimposed over an antiferromagnetic phase. We present the variation of retentivity versus temperature in Fig. 5. The remanent magnetization is seen to increase below 100 K suggesting development of a small ferromagnetic component. As the spin-reorientation effects are characteristic features of the orthoferrite compounds in which the spins rotate from one crystallographic direction to another in a continuous manner, indicative of a second-order phase transition [54,55], such scenario can also provide a possible explanation to the magnetization data of the NFMO presented above. However, it is very difficult to conclude about the type of magnetic structure and nature of spin reorientation based on the average magnetization data alone. Transition occurs most probably from one type of antiferromagnetic order to another type having a weak ferromagnetism below 100 K. Further, microscopic analysis of magnetic structure is required to completely understand the magnetic properties of NFMO as discussed in the following section.

2. Neutron diffraction and depolarization measurements

In this section, a systematic evolution of the NFMO magnetic structure based on neutron diffraction data has been discussed. In Fig. 2, we have already seen the neutron diffraction pattern at 300 K, with a broad hump corresponding to short-range magnetic ordering centered at $2\Theta = 16^\circ$($\lambda = 1.2443$ Å), which indicates presence of the magnetic correlations even above T_N.

We now present in Fig. 6, the temperature dependent neutron diffraction measurements which have been performed at PD-I ($\lambda = 1.094$ Å). As temperature is lowered below 250 K,

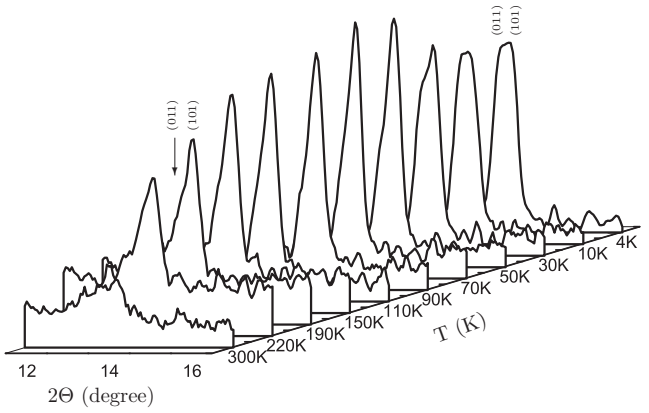

FIG. 6. Evolution of magnetic peak in neutron diffraction data as a function of temperature. These temperature dependent measurements were performed at PD-I ($\lambda = 1.094$ Å).

a clear magnetic Bragg peak is observed at ∼14.2°, which is convolution of (011) and (101) peaks. The nuclear Bragg reflections due to the two peaks are forbidden in the *Pbnm* space group. However, their magnetic reflections have non-zero structure factors. This further confirms 250 K as the value of T_N, which is also suggested by magnetization measurements in previous section. Intensity of the magnetic peak increases and (011) peak occurs at a lower angle in the form of shoulder hump on the total magnetic Bragg peak down to 70 K. The intensity ratio of the two peaks $[I(011)/I(101)]$ is approximately $\frac{1}{3}$ at 70 K suggesting a G-type antiferromagnetic structure with spins aligned along the y direction [11]. The spectral weight of the (101) peak shifts to the (011) peak below 70 K and the ratio of both peaks becomes equal close to 4 K, which represents a G-type antiferromagnetic structure with spins aligned along z direction [11]. Such temperature-induced changes in the magnetic peaks clearly stipulate a spin reorientation below 70 K. However, it is not possible to completely resolve both the peaks at the incident neutron wavelength of 1.094 Å due to the resolution limit of the instrument (PD-I).

The systematic evolution of the $I(011)/I(101)$ is better understood with neutron diffraction experiments performed at D1B(CRG) using a wavelength of 2.524 Å between 90 and 1.5 K. At this higher wavelength (2.524 Å), the magnetic Bragg peaks (011) and (101) are well resolved. Further detailed analysis has been performed on low-temperature neutron diffraction data (from D1B) to quantify the magnetic structure and temperature induced spin reorientation in NFMO. In Table II, magnetic moments along with other parameters of NFMO (as derived from D1B data) and other orthoferrites (pure as well as substituted) are listed.

The ordering vector in NFMO is $k = (0,0,0)$, which is same for the two end compounds, indicating that the magnetic and structural unit cells are identical. Comparison of the diffraction pattern with the two end compounds suggests that the antiferromagnetic ordering is identical with G-type $NdFeO_3$ rather than the A-type $NdMnO_3$.

To obtain the detailed spin configuration in a unit cell, refinement of the magnetic structure has been performed for the data collected from D1B(CRG) at 90, 50, 36, 15, and 1.5 K (Fig. 7). These five temperatures cover entirely the reorientation transition region. Since Mn and Fe occupy the same 4*b* site in NFMO, therefore Fe-Mn ordering is identical. On the other hand, Nd occupies 4*c* site and thus can order independently, however, in conjunction with the Fe-Mn ordering.

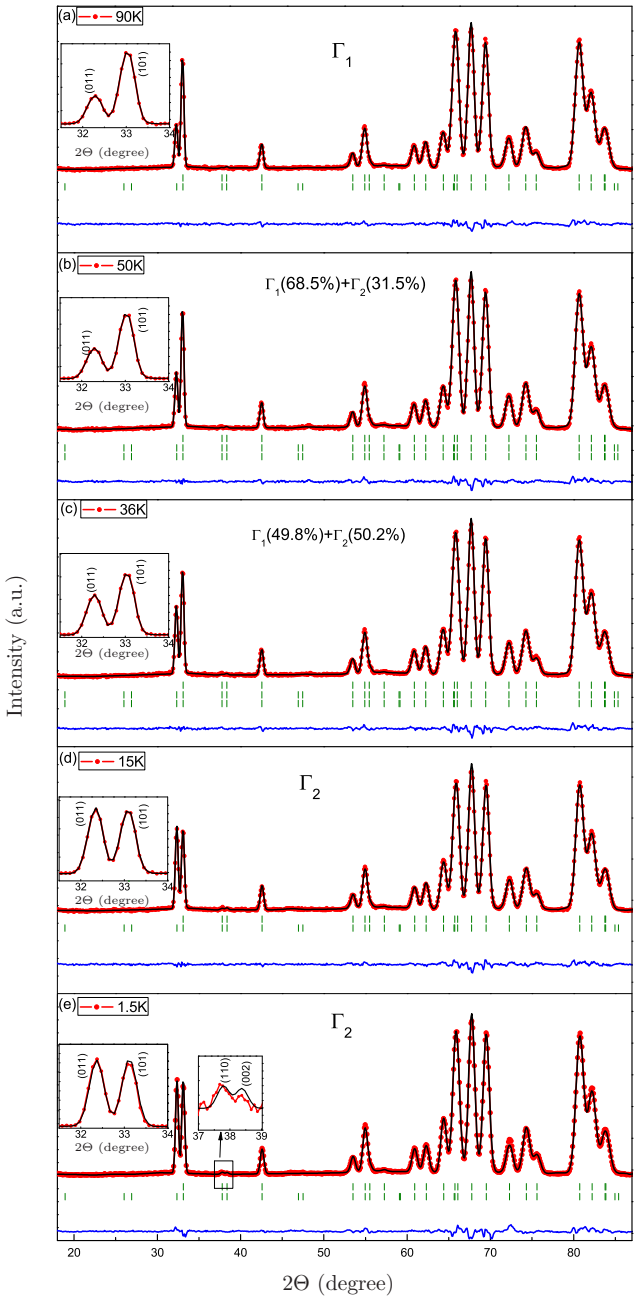

FIG. 7. Experimental and refined neutron diffraction patterns of NFMO for various temperatures from 1.5 to 90 K measured at D1B(CRG). Inset shows the changes in the magnetic Bragg peak as a function of temperature. Inset in (e) Weak magnetic signal at 38° due to Nd magnetism (F_x).

For experimentally determined magnetic ordering vector $k = (0,0,0)$, there exists eight irreducible representations, Γ_1 to Γ_8. Four out of these eight representations correspond to zero coefficients. Thus we consider four irreducible representations Γ_1 to Γ_4 which correspond to the Shubnikov magnetic space groups, Γ_1 ($Pbnm$), Γ_2 ($Pbn'm'$), Γ_3 ($Pb'nm'$), and Γ_4

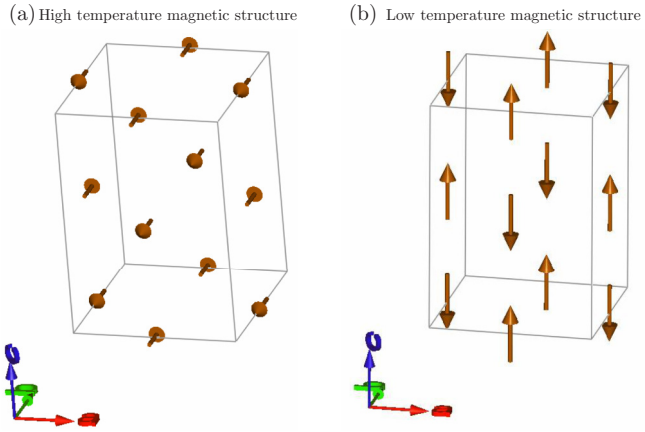

FIG. 8. Magnetic structure of NFMO represented by (a) Γ_1 space group at $\gtrsim$70 K and (b) Γ_2 space group at 4 K.

($Pb'n'm$). Using Bertraut's notation [56], these four magnetic space groups can be written in a simplified manner as $A_xG_yC_z$, $F_xA_yG_z$, $C_xF_yA_z$, and $G_xC_yF_z$, respectively, corresponding to magnetic ordering of the Cartesian components of M^{3+} spins in the unit cell. A- and C-type antiferromagnetic ordering is due to hidden canting of the spins, while F_x is due to overt canting of spins corresponding to a ferromagnetic component. A- and C-type antiferromagnetic orderings are not observed experimentally in present study probably due to small magnitude of the overt and hidden angles and have not been discussed further. Corresponding to Γ_1, Γ_2, Γ_3, and Γ_4 representations, Nd spins can order as C_z, F_xC_y, C_xF_y, and F_z, respectively [54].

At 90 K [Fig. 7(a)], the best fit is obtained for Γ_1 representation, i.e., the G_y structure. The spins point in the y direction and the M atoms in the unit cell arrange as G-type antiferromagnet as shown in Fig. 8(a). Also we do not observe any ferromagnetic component due to canting of the spins in accordance with Γ_1 representation. Thus in NFMO, below T_N, the magnetic structure belongs to the Γ_1 representation with the y direction as easy axis, unlike the usual trend observed in orthoferrites (pure as well as substituted ones (at R or M sites) in which the first magnetic ordered structure belongs to Γ_2(with moment along x direction) or Γ_4 (with moment along z direction) representations. Few orthoferrites, for instance, $Dy_{0.5}Pr_{0.5}FeO_3$, attain magnetic structure represented by the Γ_1 in the low-temperature phase after a spin reorientation transition from Γ_4 (high-temperature phase) [57]. In $TbFe_{0.5}Mn_{0.5}O_3$, the Γ_1 phase develops below spin reorientation transition temperature (low-temperature phase) as a co-existing phase with the high-temperature Γ_4 phase (see Table II) [54]. Similarly in $DyFeO_3$, the Γ_1 phase is attained below 35 K [58]. Thus the Γ_1 phase can be attributed to the large single ion anisotropy of RE ions in Dy and Tb based orthoferrite compounds. However, in NFMO, the Γ_1 phase seems to be the preferred magnetic ordering at high temperature (above spin reorientation temperature) itself. Since the single-ion anisotropy of Nd is much smaller and could be neglected in this high-temperature region, the development of Γ_1 phase can be attributed to the single ion anisotropy of Mn ion. The Hamiltonian corresponding to single ion anisotropy term of Mn/Fe ions is given by DS_z^2-$E(S_x^2 - S_y^2)$, where D and E are anisotropic constants. The necessary condition for stability of Γ_1 structure is $E > 0$ and $D > -E$ [9].

Though Fe and Mn ions are in the 3+ oxidation state, the total wave function of Fe^{3+} ($S = 5/2$) has A_{1g} symmetry, which is S-like and hence isotropic. On the other hand, in Mn^{3+} ($S = 2$), the total ground-state wave function is E_g-type, which is highly anisotropic. From electron spin resonance studies of transition metal octahedral complexes, it is found that the values of D and E in Mn^{3+} complexes are almost two orders of magnitude larger than that in Fe^{3+}complexes [59]. Thus the easy axis of magnetization of Fe/Mn sublattice is decided by the large single ion anisotropy of Mn^{3+} ion. To the best of our knowledge, this is first report of antiferromagnetic ordering with Γ_1 representation above spin reorientation transition temperature (high-temperature phase) in orthoferrites.

At 50 K [Fig. 7(b)], an increase in the ratio of intensities of the (011)/(101) peaks is observed, indicating the process of ongoing reorientation. At this temperature, the magnetic structure is best refined by a mixture of Γ_1 and Γ_2, wherein the two phases exist in a ratio of 68.5:31.5, respectively. The Γ_2 representation, corresponding to F_xG_z spin structure [as shown in Fig. 8(b)], has the z component as the major spin component unlike the easy y direction in Γ_1. Similar to Γ_1, the M sublattice spins also order as G-type in Γ_2 representation. At 36 K, the diffraction pattern is best fitted to combination of Γ_1 and Γ_2 occurring in the ratio of 49.8:50.2 [Fig. 7(c)]. From Table II, a gradual decrease in the y component of magnetic moment is observed, while there occurs a corresponding increase in the z component.

Finally, as shown in Figs. 7(d) and 7(e) for 15 and 1.5 K, respectively, intensities of both the magnetic peaks are comparable which suggest the existence of only one magnetic phase, i.e., Γ_2 at low temperatures. This also confirms the fact that the z component of spins are aligned as G-type antiferromagnet. The refinements for 15 and 1.5 K as shown in Figs. 7(d) and 7(e) confirm that the magnetic structure entirely belongs to Γ_2 representation at these temperatures. At 1.5 K, the maximum magnetic moment of 2.42(3) μ_B is obtained from the analysis, which is comparable to the value (2.2 μ_B) estimated by Troyanchuka *et al.* [34].

At 1.5 K, we observe development of an additional weak magnetic signal at 38.2°, which is due to the ferromagnetic component of the Γ_2 representation. Hence the refinement was carried out assuming ordering of Nd spins in the Γ_2 representation corresponding to F_xC_y arrangement, which yields a magnetic moment to 0.13 μ_B. However, magnetic Bragg peaks of C_y component are not observed, which should occur at 25°. Thus the absence of antiferromagnetic ordering (C_y arrangement) suggests that the nature of Nd ordering is ferromagnetic only. This is unlike the case of the $NdFeO_3$, which has antiferromagnetic ordering (C_y) with a moment value of $\sim$1 μ_B (see Table II). In $NdMnO_3$, the ferromagnetic component (without any antiferromagnetic ordering) of Nd develops in the z direction with a relatively high value of 1.2 μ_B as mentioned in Table II. The observed value of Nd magnetic moment (0.13 μ_B) lies within the range of magnetic moments revealed from the DC magnetization data at low temperature. Though the ferromagnetic peak could also arise due to canting of Fe/Mn spins, the observed value of 0.13 μ_B

TABLE II. Magnetic structural details and transition temperatures of $NdFe_{0.5}Mn_{0.5}O_3$ from present studies and comparison with literature for end compounds $NdMnO_3$, $NdFeO_3$ and related compounds. We list the three magnetic moment components along with rare earth moment M_R, and the corresponding representations for various temperatures.

Compound	T_N(K)	Spin reorientation		Magnetic moment(μ_B)							
		Range	IR	M_x	M_y	M_z	$\|M\|$	M_R	χ^2	T (K)	Reference
$NdFe_{0.5}Mn_{0.5}O_3$	250	60-30	$\Gamma_1 \rightarrow \Gamma_2$	–	2.22(1)	–	2.22(1)	–	3.83	90	This work[a]
				–	2.07(2)	0.96(6)	2.27(3)		3.80	50	”
				–	1.62(3)	1.63(3)	2.29(3)		3.99	36	”
				–	–	2.32(1)	2.32(1)	–	3.86	15	”
				–	–	2.42(3)	2.42(3)	0.13(5)	6.86	1.5	”
				–		–	±0.9		1.92	290	[34]
				–		–	±2.2		2.72	4.3	[34]
$NdFeO_3$	690	160-70	$\Gamma_4 \rightarrow \Gamma_2$	3.84(5)	–	0.46(48)			1.58	290	[20]
				1.24(15)	–	3.96(5)	4.14(9)	1.10(7)[b]	1.76	1.5	[20]
$NdFeO_3$(single crystal)				–	–	–		0.9(2)[c]	–	0.5	[19]
$NdMnO_3$	78	–	Γ_5	2.80(3)	−1.08(12)	–	3.00(7)	–	1.3	21	[44]
$NdMnO_3$	”	–	”	2.89(3)	−1.44(18)	–	3.22(9)	−1.2(18)	1.3	1.5	[44]
$NdMnO_3$	73	15	”	2.44(1)	−1.66(6)	–	2.95(7)	−1.06	–	1.5	[30]
$TbFe_{0.5}Mn_{0.5}O_3$	295	35-25	$\Gamma_4 \rightarrow \Gamma_1 \rightarrow \Gamma_4$	–				0.6(2)		2	[54]
$YFe_{0.55}Mn_{0.45}O_3$	365	300	$\Gamma_4 \rightarrow \Gamma_1$	1.51(2)	–	0.29(9)			4.01	340	[60]
				–	3.43(2)	0.16(10)			5.46	2	[60]

[a]Measurements performed at D1B(CRG).
[b]Corresponds to C_y component of Nd ordering.
[c]Corresponds to C_y component of Nd ordering.

is one order of magnitude higher compare to the moment arising due to DM interaction between canted spins of Fe/Mn ions. This value of the magnetic moment, the large remanent magnetization, and coercivities from M-H loops indicate a role of the ferromagnetic polarization of the Nd^{3+} sublattice in spin reorientation process of Fe/Mn spins.

To establish the presence of ferromagnetic component further, the depolarization of incident polarized neutrons transmitted through the sample was checked. It may be noted that the incident neutron beam should not get depolarized for antiferromagnetic ordering. Figure 9 shows temperature dependence of the flipping ratio of polarized neutron spins. It remains constant down to ∼75 K, below which it decreases slowly. The observed decrease in the flipping ratio confirms the presence of ferromagnetic correlations, as observed in the magnetization and neutron diffraction study. The slow decrease in the flipping ratio with temperature agrees well with neutron diffraction measurements where the volume fraction of the magnetic phase Γ_2 increases with decreasing temperature. It means that the volume fraction of the Γ_2 phase is directly correlated with the ferromagnetic component of the sample.

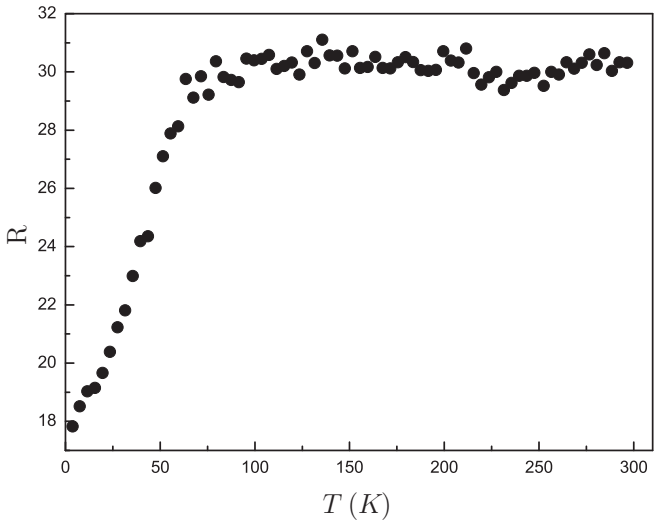

FIG. 9. Temperature variation of flipping ratio (R) under an applied magnetic guide field of 50 Oe for NFMO. Polarized neutron spectrometer was used for the measurement.

From the neutron diffraction and depolarization measurements, we can conclude that an antiferromagnetic G-type ordering exists below 250 K in the Γ_1 irreducible representation with spins aligned along y axis. The magnetic ordering in Γ_1 representation does not have any associated weak ferromagnetism due to canting of the spins. Spins start to reorient below 75 K and a new magnetic phase with Γ_2 representation appears in combination with Γ_1. An associated weak ferromagnetism also appears correlated to the Γ_2 phase. This is very clearly evident from the magnetization and depolarization measurements. The spin reorientation transition completes below 25 K and only one phase with Γ_2 (F_xG_z) representation exists having G_z antiferromagnetic ordering and a weak ferromagnetic component due to Nd spins.

IV. PHENOMENOLOGICAL EXPLANATION OF SPIN REORIENTATION

The process of reorientation, which is common to all orthoferrites, arises due to rotation of easy axis of magnetization with temperature or external magnetic field. Initially, it was believed that the temperature variation of anisotropic constants alone can be responsible for the spin reorientation.

Horner *et al.* [61] explained the reorientation process in terms of variation of easy axis as a function of temperature by means of a simple Hamiltonian $H = K_1\sin^2\theta + K_2\sin^4\theta$, where K_1 and K_2 are the temperature-dependent anisotropic constants and θ is the angle of easy axis rotation. However, it was found later on that the antisymmetric and anisotropic symmetric exchange interactions between R and M spins are primarily responsible for the reorientation process [9]. In the parent compound $NdFeO_3$, the spin reorientation occurs in the ac plane (i.e., the easy axis moves from a to c direction in a continuous manner between temperatures T_2 and T_1 below T_N). However, in NFMO, we observe the spin reorientation to happen in the bc plane resulting in the rotation of easy axis from b to c direction, between 75 and 25 K.

The complete spin configuration of NFMO in high-temperature phase can be denoted as $\Gamma_1(A_x,G_y,C_z;C_z^R)$. In this configuration, there is no ferromagnetic component of magnetic ordering. At low temperatures below spin reorientation, the magnetic ordering can be described as $\Gamma_2(F_x,C_y,G_z;F_x^R,C_y^R)$, which has ferromagnetic components. Therefore the reorientation region can be depicted as $\Gamma_{12}(A_x,G_y,C_z,F_x,C_y,G_z;F_x^R,C_y^R,C_z^R)$ [9]. Thus in NFMO, the easy axis of the M spins rotates continuously in the bc plane during spin reorientation. We define a rotation angle θ, which describes the rotation of the easy axis. In the spin reorientation region, let θ correspond to the angle of rotation of the easy axis in the bc plane, which varies between 0 and $\pi/2$ as the temperature is varied. Similar to the analysis given by Yamaguchi [9], one can understand the process of reorientation by means of effective fields acting on the M^{3+} spins generated by the anisotropic Nd-M interactions. The effective fields due to isotropic Nd-M interactions do not intend to change the magnetic symmetry. Below a certain temperature, θ starts increasing, and the terms proportional to $\sin\theta$ in free energy expression become nonzero. As a result, new anisotropic effective fields develop on M^{3+} spins, which are proportional to the antisymmetric Nd-M interactions. Due to these interactions, developed effective fields act along the z direction on the M^{3+} spins. Thus the sublattice magnetization undergoes rotation in order to align parallel to the new effective field along z direction keeping the antiferromagnetic configuration. In the following section, we will show through *ab initio* total energy calculations, how the Nd-M interaction is indeed responsible for the spin reorientation process in NFMO.

V. ELECTRONIC STRUCTURE

Due to complex magnetic behavior arising out of the interplay between the Mn^{3+} and Fe^{3+} ions as evident from the experimental observations discussed above, we attempt to evaluate the ground-state magnetic order of the system and the associated spin reorientation phenomenon in a systematic manner using first-principles density functional theory calculations. Complete random distribution of Mn and Fe ions within the orthorhombic unit cell of NFMO will require a very large supercell, which will be computationally very expensive. Therefore we have considered three possible structural configurations of Mn and Fe ions, which are labeled as (001), (110), and (111)-cationic ordering. Figure 10 depicts these three structures. In the (001) ordering, the Mn and Fe

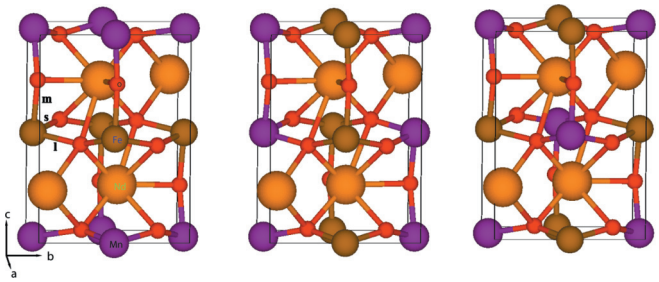

FIG. 10. Three possible structural configurations of Fe and Mn ions considered in our calculations: (001) (left), (110) (middle), and (111) (right), respectively.

planes are alternately arranged along the c direction. In the (110) arrangement, Mn and Fe ions are alternately arranged in the ab plane and the same arrangement is repeated along the c direction, while in the (111) arrangement Mn and Fe ions are alternately arranged along all the three directions.

For each of these three cationic arrangements, structural optimisation of the orthorhombic unit cell have been performed within GGA where the ionic positions were relaxed keeping lattice parameters fixed at their experimental values. These three structures were further optimized for various collinear magnetic orderings viz. ferromagnetic, A, C, and G-type antiferromagnetic orderings within the unit cell. Since our experimental studies show a G-type magnetic ordering, the structural parameters have been listed in Table III obtained for the three cationic orderings only for the G-type magnetic arrangements. Experimentally, Mn-O and Fe-O bond lengths could not be determined individually whereas in our relaxed structure, we obtain different bond-lengths for Mn-O and Fe-O. The MnO_6 shows maximum inequality in the bond lengths in the case of (001) cationic ordering similar to $NdMnO_3$. Thus among the three possible Mn/Fe arrangements, (001) shows maximal effect of J-T distortion at Mn site.

With the optimized structural parameters, GGA+U calculations for various U values are performed. The relative energies of three cationic (Fe/Mn) arrangements along with four magnetic orderings within GGA+U ($U = 6.95$ eV and $J = 0.95$ eV) are listed in Table IV, considering the FM order in (001) structure to be at zero. Overall energy comparison shows that the G-type magnetic order [for (001) Fe/Mn arrangement] is the ground state, which is consistent with our experimental observations discussed in previous sections. We now discuss the role of Coulomb correlation U on the ground-state electronic structure and magnetism for all the three cationic orderings. Using the relaxed structural

TABLE III. Relaxed structural parameters of NFMO with G-type magnetic ordering within GGA.

Mn/Fe arrangement	(001)	(111)	(110)
Fe-O1	2.0423	2.0349	1.9826
Fe-O2	1.9964	2.0657	2.05558
Fe-O2	2.0250	2.0358	2.0838
Mn-O1	1.93196	1.9407	1.9274
Mn-O2	1.92113	1.9501	1.9478
Mn-O2	2.10256	1.9825	1.9592

TABLE IV. Relative energies (in meV) for various magnetic configurations within GGA+U ($U = 6.95$ eV and $J = 0.95$ eV) for the three possible Mn/Fe cationic ordering.

Magnetic ordering	(001)	(110)	(111)
FM	0	349	687
A	−71	450	229
C	−145	187	−107
G	−458	298	50

coordinates, the self-consistent calculations were performed for various values of $U_{\text{eff}} = U - J$ in the range 0 to 6 eV. The values of U and J were kept identical for Mn and Fe. In absence of correlation, the Mn and Fe magnetic moments are observed to be much smaller than 4 μ_B and 5 μ_B expected from Mn^{3+} and Fe^{3+}, respectively, for all the magnetic orderings. For instance, in the G-type magnetic ordering, Mn and Fe show magnetic moment values of 3.2 μ_B and 3.6 μ_B respectively. This can be due to the hybridization between the $3d$ states of Mn and Fe with O $2p$ states. Furthermore, in the absence of correlations, the density of states (DOS) also show a half-metallic behavior for all the cationic and magnetic orderings. On incorporating Coulomb correlation, the ground-state magnetic configuration undergoes a variation which also depends on the Mn/Fe ordering in the unit cell. In the case of (001) arrangement, the G-type magnetic ordering emerges as the minimum energy state till a maximum value of $U_{\text{eff}} = 6$ eV. In the case of (111) arrangement, it is found that till $U_{\text{eff}} = 2.5$ eV, the G-type magnetic ordering remains as ground state. However, with further increase in U_{eff}, the C-type magnetic ordering becomes the minimum energy state. In the case of (110) cationic arrangement, the C-type always remains the ground state for all values of U_{eff} with the G-type remaining in close proximity. Thus the role of correlations in stabilizing the G-type magnetic ordering occurs probably for smaller values of U_{eff}. This is unlike the theoretically studied double perovskite Ho_2MnFeO_6, in which the correlations affect structural and electronic behavior, but the magnetic ordering is not affected by the presence of correlations [32].

Figure 11 shows the partial spin-polarized DOS of Mn and Fe for the three Fe/Mn arrangements with $U_{\text{eff}} = 6$ eV. It is clear from the DOS that Mn ions exist in the high spin 3+ valence state. The e_g states of Mn split around the Fermi level due to the J-T effect as discussed above. On the other hand, Fe ions also remain in high spin 3+ valence state with a large exchange splitting between majority and minority states pushing the fully filled majority spin states to an energy range far below (∼8 eV) Fermi energy. Therefore the overlap between Mn and Fe states is seen to be much reduced and the band gap is solely decided by the J-T splitting of Mn e_g states. The band gap is observed to be the highest (i.e., around 1 eV) for (001) ordering whereas it is around 0.3 eV for (111). The (110) ordering gives rise to a very small gap. In case of (001) ordering, a co-operative J-T effect exists in addition to the local J-T effect in the Mn planes, which gives rise to a long-range orbital ordering in Mn plane similar to $NdMnO_3$ (i.e., alternate arrangement of $d_{3x^2-r^2}$ and $d_{3y^2-r^2}$ at neighboring Mn sites). This orbital ordering gives rise to an enhanced band gap in this case. It is also interesting to note at this point that

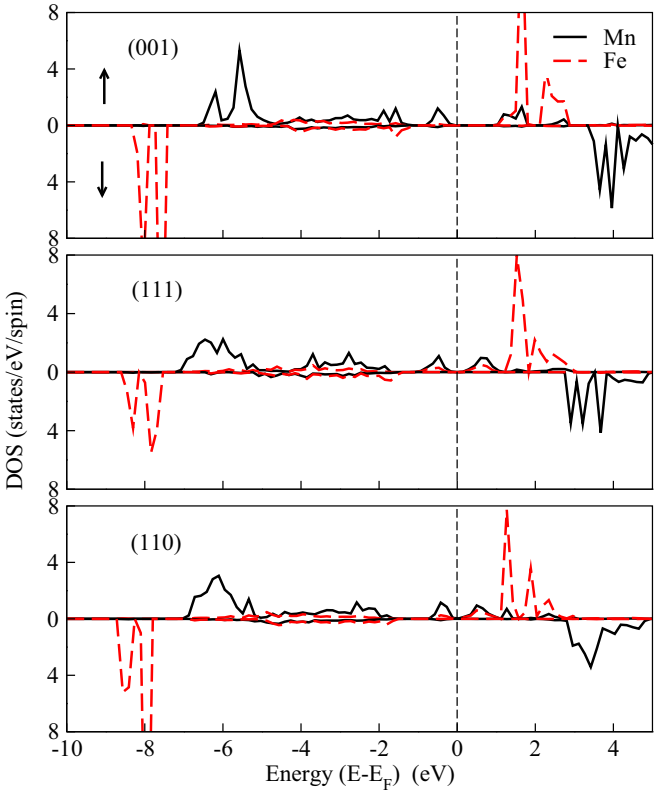

FIG. 11. Spin-polarized DOS of Mn and Fe for the three cationic orderings within GGA+U ($U = 6.95$ eV and $J = 0.95$ eV).

due to very less overlap between Fe and Mn states in all the three ordering, the exchange interaction between Fe and Mn would be weaker in comparison to Mn-Mn and Fe-Fe exchange in NFMO. This is one possible reason for (001) (where Mn and Fe ions are segregated in separate ab planes along c direction) to come out as the lowest energy state. Finally, in order to understand the mechanism of experimentally observed spin reorientation from high-temperature Γ_1 phase to low-temperature Γ_2 phase, we carried out calculations with noncollinear arrangement of spins and considered the spin-orbit interaction within GGA+U+SO approximation. For the high-temperature Γ_1 phase, the corresponding experimental structure with optimized ionic positions was considered. As ordering of Nd moments is not expected/observed in the high-temperature phase, the Nd $4f$ moments were kept frozen in the core states and Fe/Mn spins were considered to form a G-type magnetic ordering among themselves. The total energies for the three situations were calculated with Fe/Mn spins pointing along a, b, or c directions. For both (111) and (001) arrangements of Fe/Mn, b direction was obtained as preferred (or easy) axis of magnetization. This result explains our experimental observation of Γ_1 magnetic phase below T_N and above 75 K (high-temperature phase). Moreover, this easy axis of magnetization along b direction is further stabilized energetically by incorporation of Coulomb correlation U. In Fig. 12(a), the total energies for different directions have been shown for (111) cationic ordering. In order to understand the role of Mn, the corresponding calculations for $NdFeO_3$ have been performed as well. In this case, it has been observed that the easy axis is a as also found to be the case in experiments

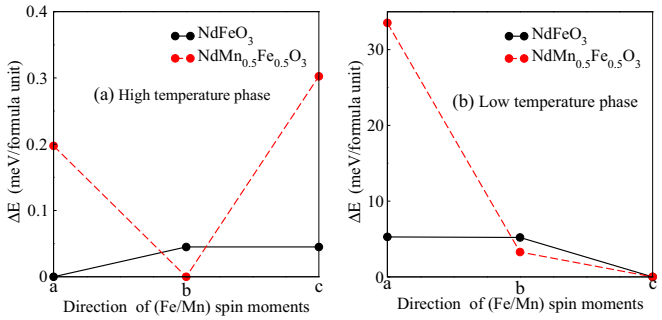

FIG. 12. Comparision of total energies for Fe/Mn spins pointing along a, b, and c directions in case of NFMO and $NdFeO_3$ for (a) high-temperature and (b) low-temperature phases, respectively.

(previously reported by Chen *et al.* [22]). Similarly, for the low-temperature Γ_2 phase (below spin reorientation transition) with G_z-type ordering, we have considered the corresponding experimental structure with optimized ionic positions and Fe/Mn spins forming a G-type magnetic ordering among themselves. However, in this case the $4f$ electrons of Nd have been treated as valence electrons and their spin moments are considered to be in C_y configuration (i.e., moments pointing along b direction are ordered in C-type AFM) as observed experimentally in case of $NdFeO_3$. Whereas in case of NFMO we had to consider F_x configuration (i.e., moments pointing along a direction are ordered ferromagnetically) rather than C_y for Nd moments to get the desired configuration obtained experimentally for Fe/Mn spins. Our results for NFMO and $NdFeO_3$ for the low-temperature phase have been presented in Fig. 12(b). It is clear from the calculations that the c direction is the preferred direction for this low-temperature phase, which is consistent with our experimental observation of Γ_2 (G_z, F_x) phase. This was also found to be the case for $NdFeO_3$ [22]. The above mentioned results indicate that Nd-Fe or Nd-Mn exchange interactions play dominant role in deciding the spin orientations of Fe/Mn spins in the low-temperature Γ_2 phase. In the high-temperature Γ_1 phase, however, the Nd moments are not ordered (net Nd moments is zero) and hence Nd-Fe/Mn exchange is absent. In this situation, magnetic anisotropy is dictated by the orbital anisotropy of Mn d orbitals.

VI. CONCLUSIONS AND SUMMARY

In summary, NFMO polycrystalline samples have been prepared and investigated in detail in order to understand its complex structural, magnetic, and electronic properties. The sample crystallizes in the space group $Pbnm$ with both Fe and Mn occupying the same crystallographic position and thus being randomly distributed in the crystal. Presence of local J-T distortion at substituted Mn sites was evident from the change in measured lattice parameters and Mn(Fe)-O bond lengths. In addition, the values of various other distortion parameters are also observed to be higher in comparison to their corresponding values for orthoferrite $NdFeO_3$, though these values are an order of magnitude smaller than those of $NdMnO_3$.

The magnetic properties of NFMO are similar to $NdFeO_3$ although with many interesting differences. The antiferromagnetic transition occurs at relatively low temperature (at 250 K) in comparison to $NdFeO_3$ ($T_N \sim 690$ K), indicating a reduction in the strength of the various exchange interactions due to Mn. Our neutron diffraction data indicate presence of short-range antiferromagnetic correlations even at 300 K, while the full ordering develops at 250 K. Unlike $NdFeO_3$, the irreducible representation of magnetic symmetry is Γ_1 below T_N with spins aligned along b direction in the G-type antiferromagnetic structure. This is highly unusual, since this magnetic representation develops at lower temperatures below the spin reorientation transition in most of the orthoferrites. The origin of this representation is attributed to the large single ion anisotropy of the Mn^{3+} ions, which is an order of magnitude larger than that of the Fe^{3+} ion. However, a competing interaction starts to become prominent between the rare-earth spins and transition metal spins, which results in a complete reorientation of the Fe/Mn spins. The reorientation occurs between 75 and 25 K with a coexistence of the two irreducible representations, Γ_1 and Γ_2. While the volume fraction of Γ_2 increases, there occurs a corresponding decrease in volume fraction of Γ_1. At the lowest temperature, the magnetic structure entirely belongs to the Γ_2 representation with G-type antiferromagnetic structure and is spin aligned along c axis. In addition, the ferromagnetic moment (F_x) due to Nd spins develops in Γ_2 phase with a value of 0.13 μ_B obtained from our Rietveld analysis. This is also concomitant with the coercivity obtained from the M-H curves, which attains a minimum value in the reorientation region. We also found evidence of ferromagnetic correlations from our neutron depolarization measurements. However, a ferromagnetic moment of 0.13 μ_B is rather large in comparison to the expected value solely from the antisymmetric interactions between Mn and Fe. This confirms the definite role of Nd^{3+} spins in reorienting the Mn and Fe spins at lower temperatures.

The process of reorientation is explained by our first-principles density functional theory calculations considering noncollinear spin arrangements within GGA+U+SO approximation. From our noncollinear calculations, we observe that in the absence of any net Nd moment, the preferred direction of Fe/Mn spins is b with G-type arrangement for high-temperature phase (below T_N). The alignment of spins changes to the c axis for low-temperature phase (below spin reorientation transition) after inclusion of Nd spins. This suggests that its the Nd $4f$-Mn(Fe) $3d$ interaction, which plays a role in reorientation of the spins at low temperature. Thus the results from our first-principles calculations corroborates further our experimental observations in understanding the complex spin reorientation process in this compound.

ACKNOWLEDGMENTS

This work was supported by the UGC-DAE Consortium for Scientific Research (CSR), Science and Engineering Research Board (SERB), and IIT Roorkee through CRS-M-228, ECR/2015/000136, and FIG-100661, respectively. A.S., A.R., and S.H. acknowledge MHRD, CSIR, and DST-INSPIRE, respectively, for their research fellowships. Authors would like to thank Prof. Sujeet Chaudhary, IIT Delhi for fruitful discussion on magnetization measurements. Authors also acknowledge the help provided by Ripandeep Singh in performing neutron diffraction experiments at PD-II, BARC, Mumbai.

[1] J. Stöhr and H. C. Siegmann, *Magnetism: From Fundamentals to Nanoscale Dynamics*, Springer Series Solid-State Science Vol. 152 (Springer, New York, 2006).
[2] G. A. Prinz, J. Magn. Magn. Mater. **200**, 57 (1999).
[3] G. A. Prinz, Phys. Today **48**, 58 (1995).
[4] L. Néel, Ann. Géophys. **5**, 99 (1949) [English version of the original reference is available in *Selected Works of Louis Néel*, edited by N. Kurti (Gordon and Breach, New York, 1988), pp. 407–427].
[5] A. Berkowitz and K. Takano, J. Magn. Magn. Mater. **200**, 552 (1999).
[6] C. H. Back and H. C. Siegmann, J. Magn. Magn. Mater. **200**, 774 (1999).
[7] A. Kimel, A. Kirilyuk, A. Tsvetkov, R. Pisarev, and T. Rasing, Nature (London) **429**, 850 (2004).
[8] J. A. de Jong, A. V. Kimel, R. V. Pisarev, A. Kirilyuk, and T. Rasing, Phys. Rev. B **84**, 104421 (2011).
[9] T. Yamaguchi, J. Phys. Chem. Solids **35**, 479 (1974).
[10] W. C. Koehler, E. O. Wollan, and M. K. Wilkinson, Phys. Rev. **118**, 58 (1960).
[11] A. Epstein and H. Shaked, Phys. Lett. A **29**, 659 (1969).
[12] R. L. White, J. Appl. Phys. **40**, 1061 (1969).
[13] H. Pinto and H. Shaked, Solid State Commun. **10**, 663 (1972).
[14] I. Sosnowska and P. Fischer, AIP Conf. Proc. **89**, 346 (1982).
[15] I. Sosnowska, E. Steichelea, and A. Hewatc, Physica B+C **136**, 394 (1986).
[16] R. Przeniosło, I. Sosnowska, M. Loewenhaupt, and A. Taylor, J. Magn. Magn. Mater. **140**, 2151 (1995).
[17] R. Przeniosło, I. Sosnowska, and P. Fischer, J. Magn. Magn. Mater. **140**, 2153 (1995).
[18] R. Przeniosło, I. Sosnowska, P. Fischer, W. Marti, F. Bartolomé, J. Bartolomé, E. Palacios, and R. Sonntag, J. Magn. Magn. Mater. **160**, 370 (1996).
[19] J. Bartolomé, E. Palacios, M. D. Kuz'min, F. Bartolomé, I. Sosnowska, R. Przeniosło, R. Sonntag, and M. M. Lukina, Phys. Rev. B **55**, 11432 (1997).
[20] W. Sławiński, R. Przeniosło, I. Sosnowska, and E. Suard, J. Phys.: Condens. Matter **17**, 4605 (2005).
[21] M. K. Singh, H. M. Jang, H. C. Gupta, and R. S. Katiyar, J. Raman Spectrosc. **39**, 842 (2008).
[22] L. Chen, T. Li, S. Cao, S. Yuan, F. Hong, and J. Zhang, J. Appl. Phys. **111**, 103905 (2012).
[23] S. J. Yuan, W. Ren, F. Hong, Y. B. Wang, J. C. Zhang, L. Bellaiche, S. X. Cao, and G. Cao, Phys. Rev. B **87**, 184405 (2013).
[24] S. Chanda, S. Saha, A. Dutta, and T. P. Sinha, Mater. Res. Bull. **48**, 1688 (2013).
[25] J. Jiang, G. Song, D. Wang, Z. Jin, Z. Tian, X. Lin, J. Han, G. Ma, S. Cao, and Z. Cheng, J. Phys.: Condens. Matter **28**, 116002 (2016).
[26] S. Y. Wu, C. M. Kuo, H. Y. Wang, W.-H. Li, K. C. Lee, J. W. Lynn, and R. S. Liu, J. Appl. Phys. **87**, 5822 (2000).
[27] R. L. Rasera and G. L. Catchen, Phys. Rev. B **58**, 3218 (1998).
[28] S. Jandl, V. Nekvasil, M. Diviš, A. A. Mukhin, J. Hölsä, and M. L. Sadowski, Phys. Rev. B **71**, 024417 (2005).
[29] T. Chatterji, G. Schneider, L. van Eick, B. Frick, and D. Bhattacharya, J. Phys.: Condens. Matter **21**, 126003 (2009).
[30] A. Kumar, S. M. Yusuf, and C. Ritter, Phys. Rev. B **96**, 014427 (2017).
[31] P. Balasubramanian, R. Yadav, H. S. Nair, H. M. Tsai, Y. Joly, J. F. Lee, S. Elizabeth, B. R. Sekhar, C. W. Pao, and W. F. Pong, Solid State Commun. **181**, 50 (2014).
[32] J. T. Zhang, X. M. Lu, J. Zhou, J. Su, K. L. Min, F. Z. Huang, and J. S. Zhu, Phys. Rev. B **82**, 224413 (2010).
[33] M. Mihalik, M. Mihalik, M. Fitta, M. Bałanda, M. Vavra, S. Gabáni, M. Zentková, and J. Briančin, J. Magn. Magn. Mater. **345**, 125 (2013).
[34] I. Troyanchuk, M. Bushinsky, H. Szymczak, M. Baran, and K. Bärner, J. Magn. Magn. Mater. **312**, 470 (2007).
[35] T. Chakraborty, R. Yadav, S. Elizabeth, and H. L. Bhat, Phys. Chem. Chem. Phys. **18**, 5316 (2016).
[36] J. Rodrguez-Carvajal, Physica B (Amsterdam) **192**, 55 (1993).
[37] H. Rietveld, J. Appl. Crystallogr. **2**, 65 (1969).
[38] E. Hovestreydt, M. Aroyo, S. Sattler, and H. Wondratschek, J. Appl. Crystallogr. **25**, 544 (1992).
[39] S. M. Yusuf and L. Madhav Rao, Pramana-J. Phys. **47**, 171 (1996).
[40] S. M. Yusuf and L. Madhav Rao, Neutron News **8**, 12 (1997).
[41] G. Kresse and J. Furthmüller, Phys. Rev. B **54**, 11169 (1996).
[42] J. P. Perdew, K. Burke, and M. Ernzerhof, Phys. Rev. Lett. **77**, 3865 (1996).
[43] V. I. Anisimov, I. V. Solovyev, M. A. Korotin, M. T. Czyzyk, and G. A. Sawatzky, Phys. Rev. B **48**, 16929 (1993).
[44] A. Munoz, J. A. Alonso, M. J. Martinez-Lope, J. L. Garcia-Munoz, and M. T. Fernandez-Diaz, J. Phys.: Condens. Matter **12**, 1361 (2000).
[45] J. A. Alonso, M. J. Martínez-Lope, M. T. Casais, and M. T. Fernández-Díaz, Inorg. Chem. **39**, 917 (2000).
[46] R. Yadav and S. Elizabeth, J. Appl. Phys. **117**, 053902 (2015).
[47] A. Anshul, R. K. Kotnala, R. P. Aloysius, A. Gupta, and G. A. Basheed, J. Appl. Phys. **115**, 084106 (2014).
[48] R. I. Dass, J.-Q. Yan, and J. B. Goodenough, Phys. Rev. B **68**, 064415 (2003).
[49] R. I. Dass and J. B. Goodenough, Phys. Rev. B **67**, 014401 (2003).
[50] F. Hong, Z. Cheng, H. Zhao, H. Kimura, and X. Wang, Appl. Phys. Lett. **99**, 092502 (2011).
[51] F. Hong, Z. Cheng, S. Zhang, and X. Wang, J. Appl. Phys. **111**, 034104 (2012).
[52] J. Lazurova, M. Mihalik, M. Mihalik Jr., M. Vavra, M. Zentkova, J. Briancin, M. Perovic, V. Kusigerski, O. Schneeweiss, P. Roupcova, K. V. Kamenev, M. Misek, and Z. Jaglicic, J. Phys.: Conf. Ser. **592**, 012117 (2015).
[53] S. Blundell, *Magnetism in Condensed Matter*, Oxford Master Series in Condensed Matter Physics 4 (Oxford University Press, Oxford, 2001).
[54] H. S. Nair, T. Chatterji, C. M. N. Kumar, T. Hansen, H. Nhalil, S. Elizabeth, and A. M. Strydom, J. Appl. Phys. **119**, 053901 (2016).
[55] H. Nhalil, H. S. Nair, Sanathkumar R., A. M. Strydom, and S. Elizabeth, J. Appl. Phys. **117**, 173904 (2015).
[56] E. F. Bertaut, in *Magnetism III*, edited by G. T. Rado and H. Suhl (Academic Press, New York, 1963).

[57] H. Wu, S. Cao, M. Liu, Y. Cao, B. Kang, J. Zhang, and W. Ren, Phys. Rev. B **90**, 144415 (2014).
[58] G. Gorodetsky, B. Sharon, and S. Shtrikman, J. Appl. Phys. **39**, 1371 (1968).
[59] R. Gerber and G. Elbinger, J. Phys. C: Solid State Physics **3**, 1363 (1970).
[60] P. Mandal, C. R. Serrao, E. Suard, V. Caignaert, B. Raveau, A. Sundaresan, and C. N. R. Rao, J. Solid State Chem. **197**, 408 (2013).
[61] H. Horner and C. M. Varma, Phys. Rev. Lett. **20**, 845 (1968).